PNAS RESEARCH ARTICLE | POPULATION BIOLOGY APPLIED MATHEMATICS

Stochastic survival of the densest and mitochondrial DNA clonal expansion in aging

Ferdinando Insalata[a], Hanne Hoitzing[a], Juvid Aryaman[a], and Nick S. Jones[a,b,1]

Edited by Mark Kirkpatrick, The University of Texas at Austin, Austin, TX; received December 15, 2021; accepted October 5, 2022

The expansion of mitochondrial DNA molecules with deletions has been associated with aging, particularly in skeletal muscle fibers; its mechanism has remained unclear for three decades. Previous accounts have assigned a replicative advantage (RA) to mitochondrial DNA containing deletion mutations, but there is also evidence that cells can selectively remove defective mitochondrial DNA. Here we present a spatial model that, without an RA, but instead through a combination of enhanced density for mutants and noise, produces a wave of expanding mutations with speeds consistent with experimental data. A standard model based on RA yields waves that are too fast. We provide a formula that predicts that wave speed drops with copy number, consonant with experimental data. Crucially, our model yields traveling waves of mutants even if mutants are preferentially eliminated. Additionally, we predict that mutant loads observed in single-cell experiments can be produced by de novo mutation rates that are drastically lower than previously thought for neutral models. Given this exemplar of how spatial structure (multiple linked mtDNA populations), noise, and density affect muscle cell aging, we introduce the mechanism of stochastic survival of the densest (SSD), an alternative to RA, that may underpin other evolutionary phenomena.

aging | mitochondria | evolution | stochastic | biomathematics

Significance

Clonal spread of DNA mutations is a fundamental phenomenon in both evolution and aging. High levels of mitochondrial DNA mutations are linked to muscle weakness in aging, which has a knock-on effect on overall health, contributing to mounting pressures on health care systems. For decades, scientists have asked how mitochondrial DNA harboring deleterious mutations can expand in skeletal muscle fibers. We provide evidence that this expansion could be driven by an unusual evolutionary mechanism, requiring only noise (stochasticity), a higher density of mutants, and a system with spatial structure. Critically, mutants need not replicate faster. This mechanism, that we have termed stochastic survival of the densest, can yield traveling waves of mutants, with potential applications in a range of evolutionary models.

The accumulation of mitochondrial DNA (mtDNA) mutations to high levels has been repeatedly linked to aging (1, 2), especially in postmitotic tissues such as neurons or muscles (3). In these tissues, a bioenergetic defect can be triggered when the proportion of mutant mtDNA in a region exceeds a threshold value (4, 5). Sarcopenia, the loss of skeletal muscle mass and strength with age, is widely associated with high levels of mtDNA with deletions (Fig. 1*A*) (6–8). A defining feature of the expansion of mtDNA deletions in muscle fibers is clonality: Damaged regions of the muscles are taken over by a single variant (8–10). The mechanism behind this phenomenon has remained unclear despite numerous authors using mathematical modeling to probe it (11–18). Some models reproduce the clonal expansion by assigning a replicative advantage (RA) to mtDNA deletions (14–18), considering them as a "selfish" genome that spreads despite being detrimental to cellular health (19, 20). Biological mechanisms to justify the supposed RA of deletions have been suggested (21–28), but for postmitotic tissues like the skeletal muscle, evidence remains equivocal (29). Moreover, there is evidence that mtDNA with deletions is preferentially eliminated (30, 31), which makes its expansion more puzzling. Neutral stochastic models have also been proposed (11–13), describing the clonal expansion in terms of neutral stochastic drift, but they require excessively high de novo mutation rates to reproduce observed mutant loads in short-lived animals (14, 32). Furthermore, most existing models neglect the spatial structure of muscle fibers. Another widely reported feature of the clonal expansion is the higher density of deletions: Regions of the muscle fiber taken over by the mutations present an approximately fivefold increase (7, 8, 33–35) in the absolute mtDNA copy number. Therefore, mtDNA deletions are the denser species, as their copy number is higher than that of wild types in the same system. Molecular mechanisms to explain the increased mutant density have been previously proposed, including the "maintenance of wild type" hypothesis (11, 36), homeostasis on adenosine triphosphate (ATP) production (37, 38), proteome status (13, 39), and copy number (40). These mechanisms essentially hypothesize that malfunctioning mutant mtDNA molecules cause an overall increase in mtDNA replication as a nuclear response to restore some compromised cellular function, such as ATP production or protein synthesis. This brings about a higher absolute number of mtDNA molecules when the proportion of mutants is higher, leading to a higher mutant density.

In this paper, we introduce a stochastic model of the spatiotemporal dynamics of mtDNA populations in skeletal muscle fibers that, consonant with data, predicts the clonal expansion of deletions without assuming any RA, even allowing mutants

Author contributions: N.S.J. designed research; F.I. and H.H. performed research; N.S.J. interpreted the results, supervised, and contributed to the analytics, statistics and computation; F.I. and H.H. analyzed data; F.I. observed and characterized the noise-induced waves, performed analytical calculations, coded the model and performed the simulations, interpreted the results, obtained new estimates of the de novo mutation rate; H.H. first investigated spatially structured systems, observed and interpreted early evidence of stochastic survival of the densest and revisited the estimates of mutant loads in muscle fibres; J.A. supported FI with mathematical techniques; and F.I., N.S.J., and J.A. wrote the paper.

The authors declare no competing interest.

This article is a PNAS Direct Submission.

[1]To whom correspondence may be addressed. Email: nick.jones@imperial.ac.uk.

This article contains supporting information online at https://www.pnas.org/lookup/suppl/doi:10.1073/pnas.2122073119/-/DCSupplemental.

Published November 28, 2022.

to be subject to preferential elimination, and drastically lowers the de novo mutation rate required to account for a given mutant load. Our analysis and results rely on the abovementioned higher density of mutants but are independent of the detailed molecular mechanism behind it. We underline that higher mutant density is not an assumption of our model but a well-established fact. The model's parameters all have a clear biological interpretation and are estimated from published experimental data.

A Minimal Model of a Counterintuitive Evolutionary Mechanism

The building block of our approach is a simple stochastic model that describes a population of mtDNA, wild type w and mutants m, evolving under central regulation by the nucleus. The main quantity of interest is the proportion of the population that is mutants, that we call heteroplasmy: $h = \frac{m}{m+w}$. This usage is accepted in the field of mathematical modeling applied to mitochondrial biology (31, 41). Importantly, we principally focus on the mechanism by which a preexisting mutation reaches high heteroplasmy through clonal expansion; we will later consider de novo mutations occurring continuously through time. The model is neutral: the two species have an identical constant degradation rate μ and an identical replication rate λ given by

$$\lambda(w, m) = \mu + c(N_{ss} - w - \delta m) \qquad [1]$$

with parameters c, N_{ss}, δ. The parameter c quantifies the strength of control exerted by the nucleus (*SI Appendix*, section 1.A). The replication rate is scaled by the distance of a count, $w + \delta m$, of the current population size from a target population N_{ss}. The parameter δ sets the relative density of mutants, whose carrying capacity is $1/\delta$ that of wild types (N_{ss}/δ against N_{ss}, see *SI Appendix*, section 1.A). For $0 < \delta < 1$, which will always be the case in this work, mutants have a higher carrying capacity and can live at higher copy numbers in the system, as observed in experimental studies referenced in the introduction (7, 8, 33–35). Therefore, mutants are denser, and this is encoded by $0 < \delta < 1$. With the above death and replication rates, a deterministic description of the system is given by the system of ODEs

$$\begin{aligned} \frac{\mathrm{d}w}{\mathrm{d}t} &= cw(N_{ss} - w - \delta m), \\ \frac{\mathrm{d}m}{\mathrm{d}t} &= cm(N_{ss} - w - \delta m). \end{aligned} \qquad [2]$$

In this setting, the system tends to the steady state $\lambda(w, m) = \mu$ (equivalently $w + \delta m = N_{ss}$), while heteroplasmy stays constant over time ($\dot{h} = 0$). More details and derivations can be found in *SI Appendix*, section 1.A.

In this work, we focus on stochastic modeling of the dynamics of mtDNA population and on the temporal evolution of mean quantities. Numerical results are obtained by averaging over multiple replicates of the dynamics of the system, simulated through the individual-based Gillespie algorithm (42) (more details in *SI Appendix*, section 1.C). A stochastic model of the single-unit system is formalized by the chemical reaction network $\{W \xrightarrow{\mu} \varnothing, M \xrightarrow{\mu} \varnothing, W \xrightarrow{\lambda} W + 1, M \xrightarrow{\lambda} M + 1\}$, where M and W stand for the (integer) number of wild-type and mutant molecules. Here, for $0 \leq \delta < 1$, mean heteroplasmy stays constant, but the mean mutant copy number increases through stochastic mechanisms. In *SI Appendix*, section 1.C, we provide derivations (see *SI Appendix*, Eqs. **S14** and **S16**) and a heuristic argument for this surprising, but long-established (11, 43, 44), behavior.

Next, we move to the stochastic two-unit model, formalized in *SI Appendix*, Eq. **S37**, that highlights the core contribution of our work. We introduce minimal spatial structure coupling two units, allowing exchange of mtDNA molecules at a per capita rate γ (see Fig. 1*B*). In each unit, there is an mtDNA population evolving under Eq. **1**. Adding spatial structure with exchange of molecules makes no difference under deterministic dynamics (Fig. 1 *C*, *Top Left*, black), makes no difference under stochastic dynamics if $\delta = 1$ (Fig. 1 *C*, *Bottom Left*, black) but crucially leads to an increase in mean heteroplasmy for stochastic dynamics with higher mutant density ($0 \leq \delta < 1$, Fig. 1 *C*, *Bottom Right*, red). This illustrates that the increase in mean heteroplasmy requires 1) spatial structure with diffusion of molecules between units, 2) stochasticity, and 3) higher density of mutants ($0 < \delta < 1$). For this reason, we term this mechanism stochastic survival of the densest (SSD): mutants outcompete wild types in a stochastic setting by virtue of being denser.

One can gain an intuitive understanding of SSD considering the limit in which the hopping rate γ is much smaller than the birth and death rates, such that the fixation time in a single unit is much less than the typical time between hops of molecules. Consider two coupled units at carrying capacity, one containing only N_{ss} wild types and the other containing exclusively N_{ss}/δ mutants ($0 < \delta < 1$). At some point, one molecule will hop to the neighboring region, and it will have time to either fix or go extinct before another hopping takes place (the low hopping rate limit). Because of the larger number of mutants, the rate of mutant hopping into the wild-type unit is higher than that of the wild type hopping into the mutant region. Likewise, because of the larger number of mutants, the fixation probability of a mutant hopping into the wild type-only unit ($1/N_{ss}$) is higher than that of a wild type entering the mutant-only unit (δ/N_{ss}). Because of the higher probabilities of hopping and fixation for mutants, the whole-system fixation probability of mutants is higher than that of wild types. In *SI Appendix*, section 3, we show that, for any value of the hopping rate, the higher whole-system mutant fixation probability is directly related to the increase in mean heteroplasmy. Therefore, the above argument gives an intuition for SSD, while also clarifying the crucial role of diffusion and higher mutant density.

In the next sections, we link SSD to the clonal expansion of mtDNA deletion mutations in skeletal muscle fibers.

Clonal Waves of Mutants in Skeletal Muscle Fibers

Skeletal muscle fibers are long, multinucleated cells, with each nucleus surrounded by a mitochondrial population under its control. The clonality of the expansion of deletion mutations (8–10) supports the idea that mtDNA molecules move along the fibers, as it is unlikely that the same mutation event occurred multiple times in distinct but adjacent regions of the same fiber. Mitochondria are tightly packed in skeletal muscle, and the mitochondrial network is hyperfused (45, 46). Moreover, it has been observed that mtDNA nucleoids move diffusively in mitochondria (47). Therefore, we assume that mtDNA molecules diffuse along muscle fibers.

We model a fiber as a chain of discrete units, each containing a nucleus and an mtDNA population notionally evolving under

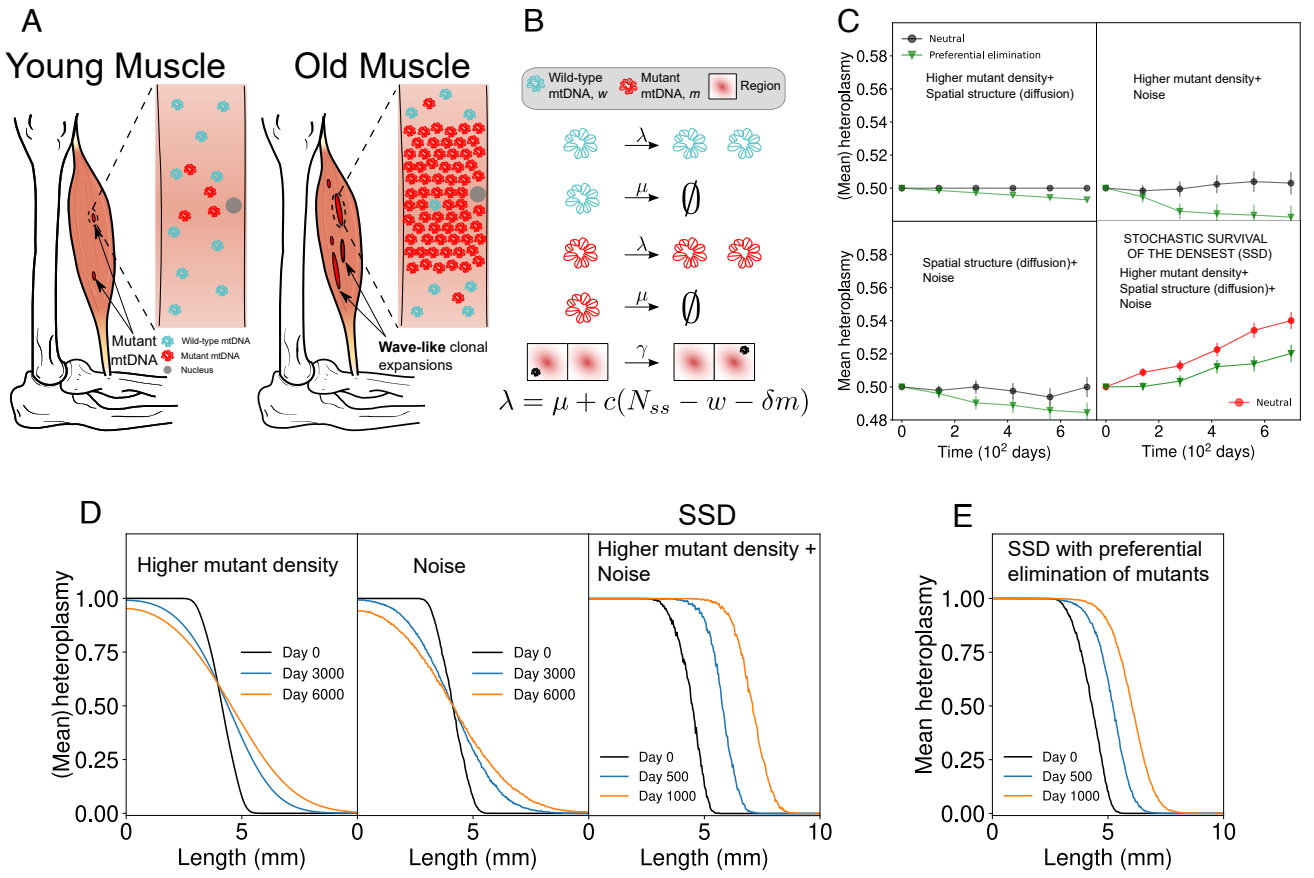

Fig. 1. Stochastic survival of the densest (SSD) can produce increases in the proportion of mutants even if they are subject to higher degradation rates than wild types. (*A*) Dysfunctional mtDNA mutants expand in muscle fibers with age in a wave-like manner, leading to defects in oxidative-phosphorylation (OXPHOS). (*B*) In a spatially extended system, the possible events are birth and death of a wild type (first two), birth and death of a mutant (third and fourth), and a mutant or wild type hops to a neighboring unit (fifth). Births happen at rate $\lambda(w, m)$ (defined at the bottom), deaths at a constant rate μ, and hopping at a constant rate γ. (*C*) SSD (bottom right subpanel) is observed in the presence of noise, spatial structure (with diffusion), and higher density of mutants, which lead to an increase in mean heteroplasmy in a neutral model (red line) and even with higher degradation of mutants (green line). If any of the factors is missing, as in the other subpanels, (mean) heteroplasmy stays constant in a neutral model (black) or decreases with preferential elimination of mutants (green). Parameters in *SI Appendix*, section 9.A. Error bars are SEM, averaged over $2 \cdot 10^3$ stochastic replicates. (*D*) In a spatially structured model (chain of units with migration), SSD drives a traveling wave of mutants only in the presence of noise and higher mutant density (rightmost subpanel), while the high-heteroplasmy front diffuses away if either noise (*Left*) or higher mutant density (*Middle*) is missing. "Length" on the horizontal axis stands for the position along the chain of units. Parameters in *SI Appendix*, section 9.A. Averaged over $2 \cdot 10^3$ stochastic replicates. (*E*) For the same model as in *D*, if mutants are preferentially degraded, an invasive wave can still occur because of SSD. If any of the three factors of SSD is missing, mutants subject to a higher degradation rate go extinct instead (*SI Appendix*, Fig. S5*B*).

nuclear control Eq. **1**. Neighboring units exchange mtDNA molecules at a constant rate γ, which models diffusion when space is discretized. In this setting, the high-heteroplasmy front diffuses away without noise (Fig. 1 *D*, *Left*) or without higher mutant density (Fig. 1 *D*, *Middle*) and advances only in the presence of noise and higher density mutants (Fig. 1 *D*, *Right*), i.e., when driven by SSD. This expanding traveling wave of mutants requires spatial structure with diffusion, noise, and higher mutant density. When these three elements are present, the wave-like expansion of mutants takes place even if mutants are preferentially degraded (Fig. 1*E*), whereas in a deterministic model, a higher degradation rate for mutants leads to their extinction (*SI Appendix*, Fig. S5*B*).

In the limit of low diffusion (hopping) considered in the previous section, one can gain an intuitive understanding of how SSD leads to a traveling wave of mutants taking over the system. In this situation, there will be a sharp separation between the mutant-only and wild type-only regions, with a step consisting of a unit containing N_{ss} wild types adjacent to a unit containing N_{ss}/δ mutants (recall $0 < \delta < 1$). Here, the higher probabilities of hopping and fixation for mutants—justified at the end of the previous section—produce a net movement of the mutant front into the wild type-only region.

SSD Matches Clonal Expansion in Muscles

Experimental data (Fig. 2*A*, 33) show the characteristic spatial profile of heteroplasmy data, with high-heteroplasmy (OXPHOS-defective) regions flanked by transition regions to low or zero heteroplasmy. This heteroplasmy profile is well described by a sigmoid (*SI Appendix*, section 18), the shape expected for a traveling wave (*SI Appendix*, section 16), compatibly with the expansion being a wave-like phenomenon. We report more profiles in Fig. 3 *A* and *C* and in *SI Appendix*, section 6.

We have estimated the speed of this expansion by analyzing data from ref. 10 on the length of abnormal regions in rhesus monkeys (see *SI Appendix*, section 17 for data processing). Regressing the lengths against age (Fig. 2*B*), we observe a relationship ($p = 5 \cdot 10^{-4}$), which is approximately linear ($R^2 = 0.76$) and corresponds to an average wave speed of (0.131 ± 0.025)μm/d. Fig. 2*C*, relative to the same fiber as in Fig. 2*A* (33), highlights the key fact (known for over 20 y

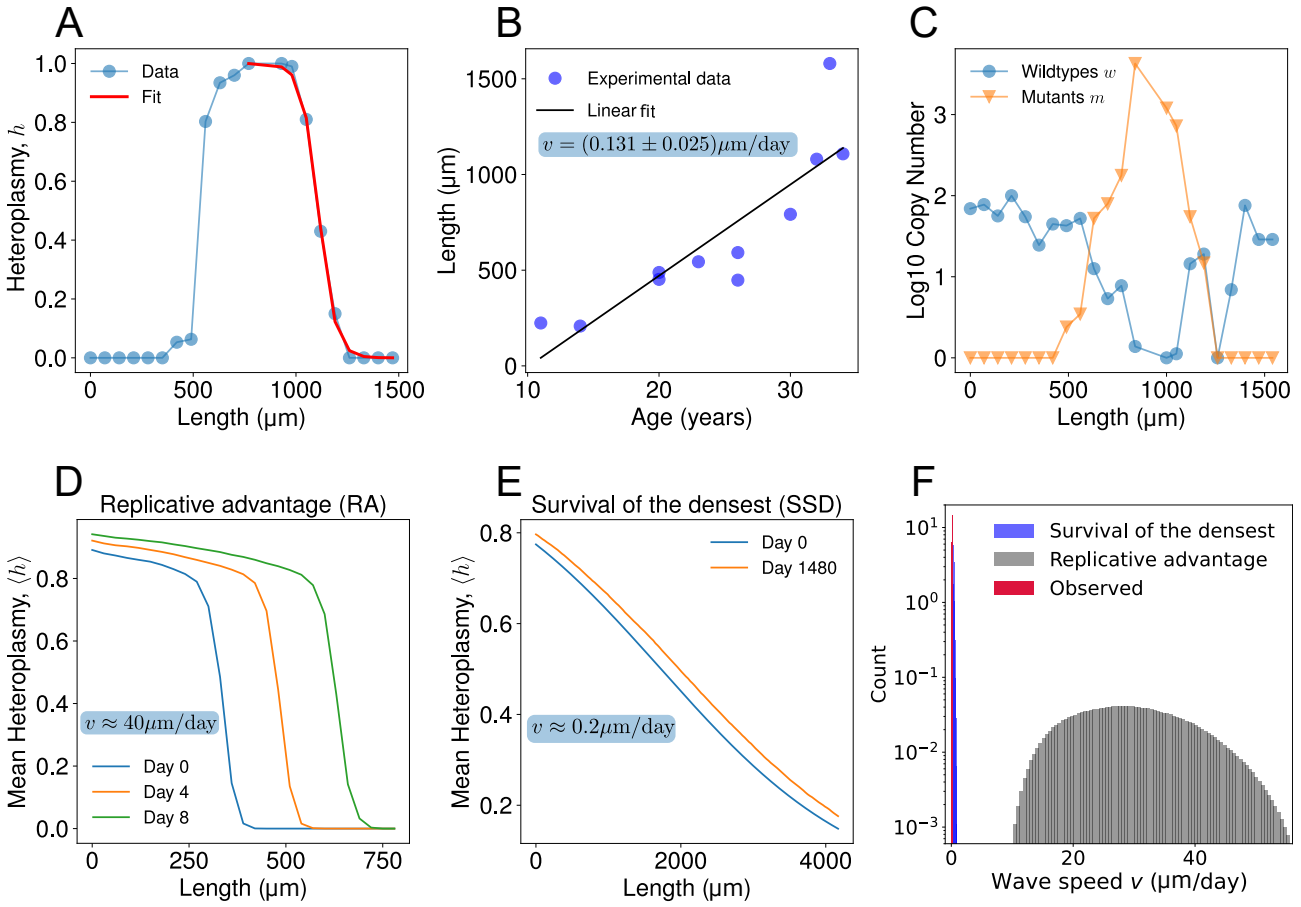

Fig. 2. Stochastic survival of the densest predicts a wave-like expansion of mtDNA mutants at a speed in agreement with experimental observations, while a standard linear replicative advantage model (*SI Appendix*, Eq. **S45**) predicts a speed a factor of ≈ 300 too large. (*A*) Spatial profile of mutant fraction (heteroplasmy) along a human skeletal muscle fiber (33). The heteroplasmy profile follows a sigmoid (*SI Appendix*, section 18), the shape expected for a traveling wave. (*B*) Experimental data on the length of abnormal regions of muscle fibers against age in rhesus monkeys, from ref. (10) (see *SI Appendix*, section 17 for data processing). An approximate linear relationship is found ($R^2 = 0.76, p = 5 \cdot 10^{-4}$), compatible with a wave-like expansion with speed $(0.131 \pm 0.025)\mu$m/d (linear fit). (*C*) Spatial structure of copy number for the wild type (blue) and mutants (orange) for the same muscle fiber as in panel *A*. The heteroplasmic regions present a higher absolute copy number, i.e., mutants are present at a higher density. (*D*) Stochastic simulations of a spatially extended model with a standard replicative advantage for mutants (*SI Appendix*, Eq. **S45**), with our best estimate of the model parameters (see *SI Appendix*, section 10) for muscle fibers of rhesus monkeys predicting a wave-like expansion with a speed of ≃ 40μm/d, 300 times faster than the observed speed. We averaged heteroplasmy on an ensemble of 500 stochastic replicates. Parameters: $\mu = 0.07$/d, $\gamma = 0.1$/d, $N_{ss} = 3500$, and $c = 2 \cdot 10^{-4}$/d, no density difference and replicative advantage $k_{RA} = 4cN_{ss}$ (see (*SI Appendix*, Eq. **S45**). (*E*) Simulations of survival of the densest yield a mutant wave speed of ≃ 0.2μm/d for the fibers or rhesus monkeys, which is comparable with experimental observations (see panel *B*). No replicative advantage and $\delta = 0.2$; other parameters are as in panel *D*. Heteroplasmy is averaged over an ensemble of 800 stochastic replicates. (*F*) Inserting probabilistic estimates of the model parameters (see *SI Appendix*, section 10) into Eq. **3**, we find that survival of the densest predicts a distribution for the wave speed (red histogram) compatible with observations (blue), whereas a wave driven by replicative advantage with the same model parameters is two orders of magnitude faster (gray).

(7, 8, 11, 34, 35)) that the absolute copy number in high-heteroplasmy regions is larger than in normal regions: Mutants are the denser species.

In *SI Appendix*, section 10, we explain our estimates of the parameter values from published experimental data for a typical mtDNA deletion mutation in rhesus monkey fibers. With these estimates, simulations of a standard linear model (*SI Appendix*, Eq. **S45**) based on RA, in which the increase in mutant density is explained by a higher replication rate as expressed in *SI Appendix*, Eq. **S46**, predict a wave-like expansion of ≈ 40 μm/d (Fig. 2*D*), 300 times faster than the observed speed. In contrast, SSD predicts a wave-like expansion of deletions with a speed of ≈ 0.2 μm/d (Fig. 2*E*).

By measuring the simulated wave speed from SSD for 110 combinations of parameters, we found that it is well described ($R^2 = 0.99$, *SI Appendix*, section 5) by the phenomenological formula:

$$v \simeq 2\sqrt{kD}, \qquad [3]$$

where D is the diffusion coefficient of mtDNA along the fibers and with $k = \sqrt{(1-\delta)^2\mu\gamma}/N_{ss}^{\frac{2}{3}}$.

Eq. **3** is analogous to the wave speed formula for the wave of advance of advantageous mutants introduced by Fisher and Kolmogorov (48, 49). In our case, k can be seen as an effective selective advantage for mutants induced by SSD, in contrast with the RA driving the original Fisher–Kolmogorov waves. In light of this analogy, our model can be seen as a reaction–diffusion system in which the reaction component emerges from the combined effect of noise and higher mutant density.

Different mtDNA deletion mutations will have different characteristics, including an increase in density or (supposed) RA. Other parameters of the system, like the diffusion constant, are also uncertain. Eq. **3** allowed us to verify robustness to uncertainty in parameter values. We obtained probability distributions for the wave speeds predicted by SSD and an RA model, by inserting draws from the distributions of parameter values (given in *SI Appendix*, section 10) into Eq. **3**, with

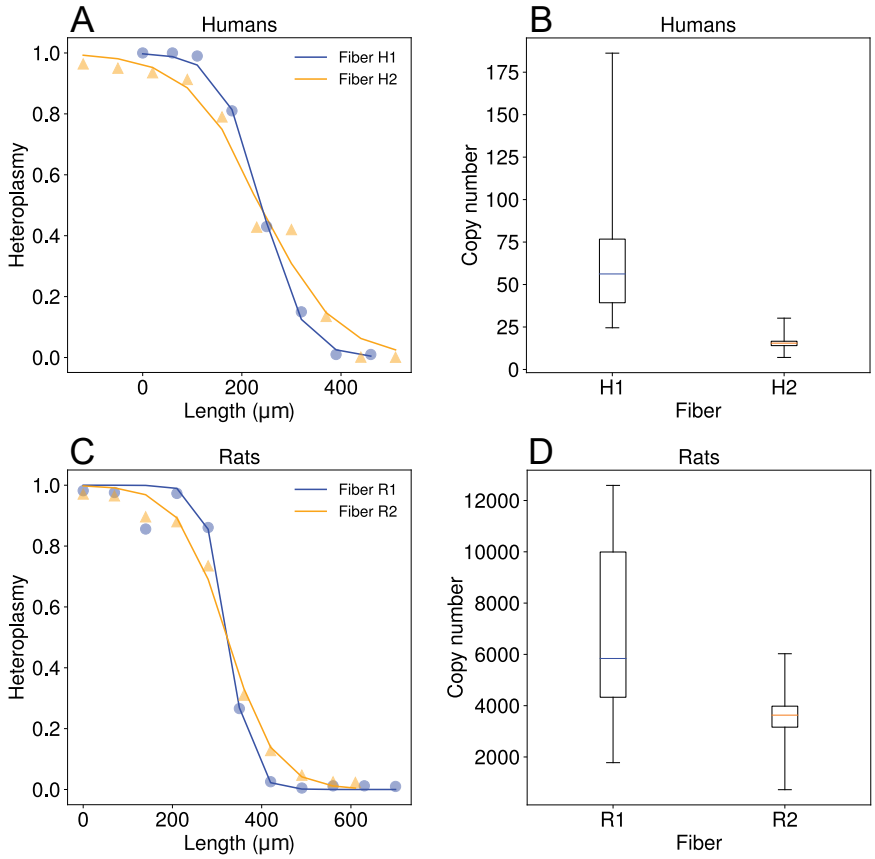

Fig. 3. A steeper wave of mutants propagates more slowly in fibers which have a higher copy number per unit length, in agreement with the predictions of stochastic survival of the densest. Data are from previous experimental studies (8, 33), our analysis is in *SI Appendix*, section 18. (*A*) Significant difference (disjoint confidence intervals) in the steepness τ of wavefronts of two human muscle fibers H1 and H2: $\tau_{H1} = (2.46 \pm 0.11) \cdot 10^{-2}$/μm, 99% confidence interval (CI) = $[2.13, 2.90] \cdot 10^{-2}$ /μm for H1 (blue, steeper) and $\tau_{H2} = (1.36 \pm 0.16) \cdot 10^{-2}$/μm, 99% CI = $[0.97, 1.99] \cdot 10^{-2}$ /μm for H2. MLE fit with curve $1/(e^{\tau x+b}+1)$ and profile-likelihood CIs; data from ref. (33). According to the mathematics of traveling waves (*SI Appendix*, section 16), the steeper wave is slower. (*B*) Comparison between the corresponding N_{ss} of the two fibers H1 and H2. We have found evidence ($p = 10^{-4}$, $d = 1.48$, one-sided Welch's *t*-test) that the average copy number per unit length (a slice of length 20 μm here) in normal regions of the two fibers H1 and H2 (N_{ss} in our model) is higher for the steeper and, hence, slower wave (H1, blue). This is in qualitative agreement with stochastic survival of the densest, which predicts that wave speed decreases with copy number. In contrast, a model based on replicative advantage predicts that speed increases with copy number. (*C*) Two muscle fibers in rats, R1 and R2, present waves of mutants with significantly different steepness τ of the waveform, as seen from the disjoint 99% CIs: $\tau_{R1} = (3.97 \pm 0.61) \cdot 10^{-2}$ /μm, 99% CI = $[2.53, 8.30] \cdot 10^{-2}$ /μm for R1 (blue, steeper) and $\tau_{R2} = (1.88 \pm 0.16) \cdot 10^{-2}$ /μm, 99% CI = $[1.46, 2.49] \cdot 10^{-2}$ /μm for R2. MLE fit with curve $1/(e^{\tau x+b}+1)$ and profile-likelihood CIs, data from ref. (8). (*D*) We have found an indication ($p = 0.06$, $d = 1.00$, one-sided Welch's *t*-test) that the average copy number per unit length in normal regions of the two fibers R1 and R2 is higher for the steeper wave (R1, blue).

the appropriate interpretation of k for the two models. The predicted distributions are plotted in Fig. 2*F*, together with the distribution of the experimentally observed wave speed obtained via linear fit (Fig. 2*B*). After accommodating this parametric uncertainty, SSD remains much superior to RA at reproducing the observed speed.

In *SI Appendix*, section 11, we show that allowing for both higher mutant death and replication rate would not change the RA wave speed distribution of Fig. 2*F*. We cannot exclude a situation in which an SSD and RA (and possibly selective elimination) coexist, but note that our analysis suggests that RA is not necessary and—on its own and in its standard form—not viable. Our null model introduces SSD and shows that it can account for the clonal expansion of mtDNA deletion mutations.

Linking Aging, Wave Speed, and Copy Number

As Eq. **3** states, SSD predicts a wave speed that decreases when copy number (per nucleus) increases. Indeed, the expansion of mutants is driven by stochastic fluctuations, whose effect generally becomes smaller for larger population size (see also *SI Appendix*, Eq. **S14**). In contrast, a standard model based on RA predicts a wave speed that increases with population size (48, 50). This allows us to test SSD and RA models against other experimental observations. It has been found that copy number depletion caused by antiretroviral therapy (51) or deficiency of the enzyme AKT2 (52) is associated with enhanced sarcopenia. Likewise, statins are well known for increasing the risk of sarcopenia (53–55) and have consistently been associated with reduction in mitochondrial copy number (56–58). Conversely, an increase in mtDNA content through exercise (59, 60) or overexpression of mitochondrial transcription factor A (TFAM) (61) and parkin (62) has been found to protect against sarcopenia and muscle atrophy.

Skeletal muscle fibers can be broadly classified into type 1 (oxidative) and type 2 (glycolytic) fibers (63). The former rely on oxidative-phosphorylation (OXPHOS) to function and typically have twice as many mitochondria as the latter (10, 64, 65), that depend on glycolysis. It is known that type 2 fibers are more affected by sarcopenia with aging (7, 10, 66–69). Small, short-lived animals like rodents show sarcopenia on a time scale

of years (from ≈ 2 y) and have a larger proportion of type 2 fibers compared to long-lived animals such as rhesus monkeys and humans (51), that exhibit sarcopenia on a longer time scale (decades). While there are other physiological differences between the fiber types, this is a further link between smaller mtDNA copy numbers and faster mutant expansion. The leading edge of a faster wave is flatter than that of a slower wave (e.g., ref. 70, summarized in *SI Appendix*, section 16). By exploiting this property, it is possible to compare the speeds of two waves by examining their shapes. Previously published data on muscle fibers for humans (33) (Fig. 3 *A* and *B*) and rats (8) (Fig. 3 *C* and *D*) show that flatter—hence faster—waves of mutants propagate along fibers with smaller copy numbers. All these observations support our model's prediction of an inverse relationship between copy number and wave speed, opposite to that predicted by a standard RA model (50).

Importantly, the traveling wave of mutants with an inverse relationship between speed and copy number is observed not only in the case of linear feedback control Eq. **1** but also for other controls encoding a higher density of mutants (see *SI Appendix*, section 15), provided that stochasticity and spatial structure (with diffusion) are present.

Low Mutation Rates Can Yield Large Mutant Loads

Previous neutral models of mtDNA dynamics in skeletal muscle fibers require high de novo mutation rates R_{mut} to explain the observed mutational loads in fibers of short-lived animals (8, 14, 32, 71). In turn, these high mutation rates produce an unrealistically high mutational diversity, at odds with the observed clonality of the expansion of deletion mutations: This shortcoming has motivated theorists to develop RA models. However, previous studies modeled skeletal muscle fibers as an unstructured bulk of well-mixed mtDNAs (12, 14, 16). Conversely, our spatially structured model exhibits SSD, that increases the probability of fixation of the denser mutants. Evidently, the R_{mut} required to explain a given mutant load is then much lower compared to models without spatial structure.

We set out to give an order-of-magnitude estimate of R_{mut} under SSD after estimating the fixation probability in a long chain of units via numerical simulations. We focused on the reciprocal of the fixation probability, as we empirically found linear relationships with N_{ss}. In Fig. 4, we plot our numerical estimate of the reciprocal of the probability that a founder mutation takes over a muscle fiber against N_{ss} over three orders of magnitude and for our best estimates of the remaining parameters (*SI Appendix*, section 10). We infer the fixation probability for $N_{ss} = 3500$ (humans (72)). Critically, we discover that fixation probability is independent of the fiber length and depends inversely on N_{ss} (a purely local parameter). In *SI Appendix*, section 13, we develop a simple argument that connects fixation probability and R_{mut}. Based on this argument, we estimate the corresponding de novo mutation rate as $R_{mut} = 4.1 \cdot 10^{-8}$–$1.6 \cdot 10^{-6}$ per replication for a typical human fiber (*SI Appendix*, section 13). This value is in line with conservative experimental estimates (12, 73) and two to three orders of magnitude smaller than estimated in the reference study (12) that neglects spatial structure (and hence SSD). In conclusion, SSD can reproduce the observed mutant loads in skeletal muscle fibers requiring drastically lower de novo mutation rates than previous neutral models.

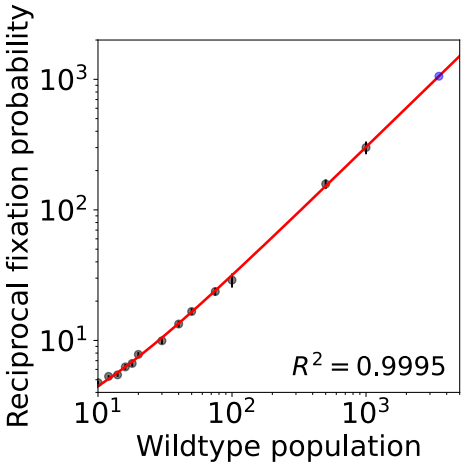

Fig. 4. Fixation probability of a founder mutation in a muscle fiber depends on local numbers of mtDNA per nucleus (N_{ss} in our model) and is independent of the total number of mtDNA in the fiber. The reciprocal of the fixation probability P_f increases linearly with N_{ss} (see *SI Appendix*, section 13), and hence, $P_f \approx \alpha / N_{ss}$, with $\alpha = (3.316 \pm 0.002)$ for $N_{ss} \gg 1$. The black dots represent estimates of this probability for $10 < N_{ss} < 1000$, obtained via stochastic simulations (details in *SI Appendix*, section 14; error bars are standard deviations). For $N_{ss} = 3500$, a plausible value for humans, the predicted fixation probability is $P_f = (9.47 \pm 0.06) \cdot 10^{-4}$ (blue dot).

Discussion

We have presented a bottom-up, physically interpretable spatial stochastic model that predicts the wave-like clonal expansion of mitochondrial deletion mutations in skeletal muscle fibers without assuming a replicative advantage (RA) and even if mutants are subject to preferential elimination. This counterintuitive effect is driven by a mechanism that we have termed stochastic survival of the densest (SSD), that depends on the stochastic nature of the model, the increased density of mitochondrial deletions (a widely observed phenomenon (7, 8, 33–35)), and spatial structure (multiple mtDNA populations with migration). As mutants are denser, in a stochastic system, a mutant is more likely to take over a less densely occupied wild type-dominated region, compared to a wild type in a densely packed mutant region. Likewise, from a densely populated mutant region, there is more frequent migration, i.e., more attempts by mutants to invade neighboring wild-type regions. These considerations help build an intuitive understanding of SSD as a mechanism whereby denser mutants can neutrally expand in a spatially structured system driven by stochastic fluctuations.

Previously, the clonal expansion of mitochondrial deletions has been modeled via an RA (14–18). We have discovered that a standard literature-parameterized linear model of this type (*SI Appendix*, Eq. **S45**) produces an expansion that is 300 times faster than observed speeds. Our model predicts instead a speed that is of the same order of magnitude as observations. We have provided a phenomenological formula for the speed of the SSD-driven wave (Eq. **3**) that has implications for therapy, since existing drugs allow us to modulate some of the parameters influencing the propagation of mutants. The SSD wave speed decreases when copy number increases, therefore, increasing copy number via interventions such as increased physical exercise (59, 60), calorie restriction (74) or both (75), and administering nicotinamide riboside (76) or niacin (77), has the potential to slow down the clonal expansion of mutants. Decreasing mtDNA diffusion (by fragmenting the mitochondrial network) or turnover seems less viable, being associated with negative consequences and health

challenges (78–80). Unlike SSD, models based on RA exhibit a speed that increases with copy number. By reviewing existing data on how copy number affects the steepness of the wavefront (which is connected to wave speed) and the likelihood of developing sarcopenia, we have corroborated the SSD-based prediction of Eq. **3** and therefore shown evidence that SSD drives the clonal expansion. Future experiments investigating the relationship between copy number and the speed of the expansion (directly or through wavefront steepness) could provide additional evidence in favor of SSD and possibly against RA. Manipulating mitochondrial turnover via administration of urolithin A (81) could also help probe Eq. **3**. Finally, we have shown that SSD lowers the de novo mutation rate needed to reproduce the observed mutant loads in humans by three orders of magnitude compared to previous models based on neutral stochastic drift (11–13).

Our core claim is that the expansion of mtDNA carrying deletions in skeletal muscle fibers is not necessarily driven by an RA or by conventional neutral drift. Rather, mutants might have an effective selective advantage induced by SSD, namely by the combined effect of stochasticity, higher density, and spatial structure with diffusion.

The expansion of mtDNA deletion mutations in skeletal muscle fibers is an experimental candidate for SSD, that might be the driving force behind other counterintuitive evolutionary phenomena. In the supplement, beyond giving a wider positioning of this work in the evolutionary literature (*SI Appendix*, sections 7–8), we show that in our model, the replication rate of all molecules increases with the proportion of mutants (*SI Appendix*, section 1.B). Therefore, each mutant brings a benefit to all other individuals in the system. Mutants' higher degradation rate might be seen as the cost of bringing this benefit (as in refs. (44, 50, 82, 83)). An altruist can be defined as an individual that benefits others at a cost to itself (82, 84), and there is thus a link between this specific definition of altruism and the mutants in our model, that prevail over wild types by adopting an altruistic strategy. Clonal expansions of mtDNA deletions in skeletal muscle fibers are obviously detrimental to cellular and organismal health, but their strategy is altruistic from the technical point of view of population dynamics, as formalized in *SI Appendix*, section 1.B. Our model may be applicable to a wider range of cells in the presence of subcellular control on subpopulations of mitochondria. Neurons might be a candidate, although their directed mitochondrial trafficking (85) is different from random diffusion. There is also evidence of exchange of mtDNA between cells (86), but the scale and nature of this in vivo are under debate. A classic setting for the wave-like spread of a trait is in the uptake of agriculture (87), which might not impart an explicit RA and might lead to higher death rates (88), but nonetheless spreads, possibly due to an increase in carrying capacity of the land. We believe that this study and the simplicity of our microscopic model might pave the way for increased recognition of SSD in evolutionary biology.

Materials and Methods

In *SI Appendix*, we provide background, explanations, and details on simulations and statistical analyses. We give a summary below.

Numerical Simulations. All original results presented in the paper are obtained by simulating a Poisson point process via the Gillespie algorithm (42). The point processes are formalized as chemical reaction networks. The single-unit system dynamics is obtained by simulating the chemical reaction network $\{W \xrightarrow{\mu} \varnothing, M \xrightarrow{\mu} \varnothing, W \xrightarrow{\lambda} W+1, M \xrightarrow{\lambda} M+1\}$, with constant degradation rate μ and replication rate λ as in Eq. **1**.

The dynamics of the two-unit system, the simplest showing SSD, is obtained by simulating two units evolving under the above dynamics and additionally exchanging molecules at a constant rate γ. Chains of units are obtained by coupling together numerous units with exchange of molecules between nearest neighbors in the chain.

Two plots (Fig. 1 *C*, *Upper Left*; Fig. 1 *C*, *Left* panel) refer to deterministic systems, modeled as systems of ordinary differential equations, as in Eq. **2** and with exchange of molecules for two or more units. These systems have been integrated numerically using the Python library SciPy.

Statistical Analyses. The sigmoidal functions in Figs. 2*A* and 3 *A* and *C* were fitted using maximum likelihood estimation (MLE) with normal likelihood. The linear fits in Figs. 2*B* and 4 were obtained via MLE, as ordinary linear least squares with normal likelihood. The distributions in Fig. 2*F* were obtained with the approach detailed in ref. (89) and can be reproduced using the online tool at http://caladis.org/ and the parameter estimates given in *SI Appendix*, section 10. The statistical test performed on the data in Fig. 3 *B* and *D* is one-tailed Welch's test (unequal-variance *t* test).

Data, Materials, and Software Availability. Previously published data were used for this work (8, 10, 33).

ACKNOWLEDGMENTS. We acknowledge Judd Aiken and Allen Herbst for advising on skeletal muscle fibers data and Sam Greenbury and Iain Johnston for useful comments about the manuscript. NJ acknowledges the Leverhulme Trust RPG-2019-408 and EPSRC EP/N014529/1. FI is supported by Imperial College's President's PhD Scholarship.

Author affiliations: [a]Department of Mathematics, Imperial College London, London SW7 2AZ, United Kingdom; and [b]EPSRC Centre for the Mathematics of Precision Healthcare, Imperial College London, London SW7 2AZ, United Kingdom

1. D. Harman, The biologic clock: The mitochondria?. *J. Am. Geriatr. Soc.* **20**, 145–147 (1972).
2. T. E. Kauppila, J. H. Kauppila, N. G. Larsson, Mammalian mitochondria and aging: An update. *Cell Metab.* **25**, 57–71 (2017).
3. N. Sun, R. J. Youle, T. Finkel, The mitochondrial basis of aging. *Mol. Cell* **61**, 654–666 (2016).
4. R. Rossignol *et al.*, Mitochondrial threshold effects. *Biochem. J.* **370**, 751–762 (2003).
5. J. Aryaman, I. G. Johnston, N. S. Jones, Mitochondrial dna density homeostasis accounts for a threshold effect in a cybrid model of a human mitochondrial disease. *Biochem. J.* **474**, 4019–4034 (2017).
6. E. Ferri *et al.*, Role of age-related mitochondrial dysfunction in sarcopenia. *Int. J. Mol. Sci.* **21**, 5236 (2020).
7. E. A. Bua, S. H. McKiernan, J. Wanagat, D. McKenzie, J. M. Aiken, Mitochondrial abnormalities are more frequent in muscles undergoing sarcopenia. *J. Appl. Physiol.* **92**, 2617–2624 (2002).
8. A. Herbst *et al.*, Accumulation of mitochondrial DNA deletion mutations in aged muscle fibers: Evidence for a causal role in muscle fiber loss. *J. Gerontol. Ser. A: Biol. Sci. Med. Sci.* **62**, 235–245 (2007).
9. C. T. Moraes, E. A. Schon, Detection and analysis of mitochondrial DNA and RNA in muscle by in situ hybridization and single-fiber PCR. *Methods Enzymol.* **264**, 522–540 (1996).
10. M. E. Lopez, N. L. Van Zeeland, D. B. Dahl, R. Weindruch, J. M. Aiken, Cellular phenotypes of age-associated skeletal muscle mitochondrial abnormalities in rhesus monkeys. *Mutat. Res. - Fundam. Mol. Mech. Mutagen.* **452**, 123–138 (2000).
11. P. F. Chinnery, D. C. Samuels, Relaxed replication of mtDNA: A model with implications for the expression of disease. *Am. J. Hum. Genet.* **64**, 1158 (1999).
12. J. Elson, D. Samuels, D. Turnbull, P. Chinnery, Random intracellular drift explains the clonal expansion of mitochondrial DNA mutations with age. *Am. J. Hum. Genet.* **68**, 802–806 (2001).
13. G. J. Capps, D. C. Samuels, P. F. Chinnery, A model of the nuclear control of mitochondrial DNA replication. *J. Theor. Biol.* **221**, 565–583 (2003).
14. A. Kowald, T. B. Kirkwood, Mitochondrial mutations and aging: Random drift is insufficient to explain the accumulation of mitochondrial deletion mutants in short-lived animals. *Aging Cell* **12**, 728–731 (2013).
15. A. Kowald, M. Dawson, T. B. L. Kirkwood, Mitochondrial mutations and ageing: Can mitochondrial deletion mutants accumulate via a size based replication advantage?. *J. Theor. Biol.* **340**, 111–118 (2014).

16. A. Kowald, T. B. Kirkwood, Transcription could be the key to the selection advantage of mitochondrial deletion mutants in aging. *Proc. Natl. Acad. Sci. U.S.A.* **111**, 2972–2977 (2014).
17. C. Lawless, L. Greaves, A. K. Reeve, D. M. Turnbull, A. E. Vincent, The rise and rise of mitochondrial DNA mutations. *Open Biol.* **10**, 200061 (2020).
18. Z. Y. Tam, J. Gruber, B. Halliwell, R. Gunawan, Context-dependent role of mitochondrial fusion-fission in clonal expansion of mtDNA mutations. *PLoS Comp. Biol.* **11**, e1004183 (2015).
19. A. Klucnika, H. Ma, A battle for transmission: The cooperative and selfish animal mitochondrial genomes. *Open Biol.* **9**, 180267 (2019).
20. J. C. Havird *et al*., Selfish mitonuclear conflict. *Curr. Biol.* **29**, R496–R511 (2019).
21. D. C. Wallace, Mitochondrial genetics: A paradigm for aging and degenerative diseases?. *Science* **256**, 628 (1992).
22. F. Diaz *et al*., Human mitochondrial DNA with large deletions repopulates organelles faster than full-length genomes under relaxed copy number control. *Nucleic Acids Res.* **30**, 4626–4633 (2002).
23. O. M. Russell *et al*., Preferential amplification of a human mitochondrial DNA deletion in vitro and in vivo. *Sci. Rep.* **8**, 1–10 (2018).
24. M. Yoneda, A. Chomyn, A. Martinuzzi, O. Hurko, G. Attardi, Marked replicative advantage of human mtDNA carrying a point mutation that causes the MELAS encephalomyopathy. *Proc. Natl. Acad. Sci. U. S.A.* **89**, 11164–11168 (1992).
25. N. Arnheim, G. Cortopassi, Deleterious mitochondrial DNA mutations accumulate in aging human tissues. *Mutat. Res. DNAging* **275**, 157–167 (1992).
26. A. D. de Grey, A proposed refinement of the mitochondrial free radical theory of aging. *BioEssays* **19**, 161–166 (1997).
27. N. Lane, Mitonuclear match: Optimizing fitness and fertility over generations drives ageing within generations. *BioEssays* **33**, 860–869 (2011).
28. W. S. Phillips *et al*., Selfish mitochondrial DNA proliferates and diversifies in small, but not large, experimental populations of caenorhabditis briggsae. *Genome Biol. Evol.* **7**, 2023–2037 (2015).
29. G. Campbell, K. J. Krishnan, M. Deschauer, R. W. Taylor, D. M. Turnbull, Dissecting the mechanisms underlying the accumulation of mitochondrial DNA deletions in human skeletal muscle. *Hum. Mol. Genet.* **23**, 4612–4620 (2014).
30. S. J. Goldman, R. Taylor, Y. Zhang, S. Jin, Autophagy and the degradation of mitochondria. *Mitochondrion* **10**, 309–315 (2010).
31. J. Aryaman, C. Bowles, N. S. Jones, I. G. Johnston, Mitochondrial network state scales mtDNA genetic dynamics. *Genetics* **212**, 1429–1443 (2019).
32. A. Kowald, T. B. Kirkwood, Resolving the enigma of the clonal expansion of mtDNA deletions. *Genes* **9**, 126 (2018).
33. E. Bua *et al*., Mitochondrial DNA-deletion mutations accumulate intracellularly to detrimental levels in aged human skeletal muscle fibers. *Am. J. Hum. Genet.* **79**, 469–480 (2006).
34. C. Barthélémy *et al*., Late-onset mitochondrial DNA depletion: DNA copy number, multiple deletions, and compensation. *Ann. Neurol.* **49**, 607–617 (2001).
35. A. E. Vincent *et al*., Subcellular origin of mitochondrial DNA deletions in human skeletal muscle. *Ann. Neurol.* **84**, 289–301 (2018).
36. S. E. Durham, D. C. Samuels, L. M. Cree, P. F. Chinnery, Normal levels of wild-type mitochondrial DNA maintain cytochrome *c* oxidase activity for two pathogenic mitochondrial DNA mutations but not for m.3243A. → G. *Am. J. Hum. Genet.* **81**, 189–195 (2007).
37. E. A. Shoubridge, G. Karpati, K. E. Hastings, Deletion mutants are functionally dominant over wild-type mitochondrial genomes in skeletal muscle fiber segments in mitochondrial disease. *Cell* **62**, 43–49 (1990).
38. P. M. Garcia-Roves, M. E. Osler, M. H. Holmström, J. R. Zierath, Gain-of-function R225Q mutation in AMP-activated protein kinase $\gamma 3$ subunit increases mitochondrial biogenesis in glycolytic skeletal muscle. *J. Biol. Chem.* **283**, 35724–35734 (2008).
39. S. A. Dogan *et al*., Tissue-specific loss of DARS2 activates stress responses independently of respiratory chain deficiency in the heart. *Cell Metab.* **19**, 458–469 (2014).
40. B. L. Gitschlag *et al*., Homeostatic responses regulate selfish mitochondrial genome dynamics in C. elegans. *Cell Metab.* **24**, 91–103 (2016).
41. I. G. Johnston, N. S. Jones, Evolution of cell-to-cell variability in stochastic, controlled, heteroplasmic mtDNA populations. *Am. J. Hum. Genet.* **99**, 1150–1162 (2016).
42. D. T. Gillespie, A general method for numerically simulating the stochastic time evolution of coupled chemical reactions. *J. Comp. Phys.* **22**, 403–434 (1976).
43. H. Hoitzing *et al*., Energetic costs of cellular and therapeutic control of stochastic mitochondrial DNA populations. *PLoS Comput. Biol.* **15**, e1007023 (2019).
44. G. W. Constable, T. Rogers, A. J. McKane, C. E. Tarnita, Demographic noise can reverse the direction of deterministic selection. *Proc. Nat. Aca. Sci.* **113**, E4745–E4754 (2016).
45. J. Avellaneda *et al*., Myofibril and mitochondria morphogenesis are coordinated by a mechanical feedback mechanism in muscle. *Nat. Commun.* **12**, 1–18 (2021).
46. B. Glancy *et al*., Mitochondrial reticulum for cellular energy distribution in muscle. *Nature* **523**, 617–620 (2015).
47. F. J. Iborra, H. Kimura, P. R. Cook, The functional organization of mitochondrial genomes in human cells. *BMC Biol.* **2**, 9 (2004).
48. R. A. Fisher, The wave of advance of advantageous genes. *Ann. Eugen.* **7**, 355–369 (1937).
49. A. Kolmogorov, I. Petrovskii, N. Piskunov, Investigation of the diffusion equation involving growth in the amount of matter, and its application to a biological problem. *Byul. Moskov. Gos. Univ. Sek. A* **1**, 1–26 (1937).
50. O. Hallatschek, Noise driven evolutionary waves. *PLOS Comput. Biol.* **7**, 1–9 (2011).
51. M. A. Pellegrino *et al*., Orthologous myosin isoforms and scaling of shortening velocity with body size in mouse, rat, rabbit and human muscles. *J. Physiol.* **546**, 677–689 (2003).
52. S. A. A. Aziz *et al*., Assessment of sarcopenia in virally suppressed HIV-infected Asians receiving treatment. *AIDS (London, England)* **32**, 1025–1034 (2018).
53. S. L. Di Stasi, T. D. MacLeod, J. D. Winters, S. A. Binder-Macleod, Effects of statins on skeletal muscle: A perspective for physical therapists. *Phys. Ther.* **90**, 1530–1542 (2010).
54. R. Ramachandran, A. S. Wierzbicki, Statins, muscle disease and mitochondria. *J. Clin. Med.* **6**, 75 (2017).
55. A. Bielecka-Dabrowa *et al*., Prosarcopenic effects of statins may limit their effectiveness in patients with heart failure. *Trends Pharmacol. Sci.* **39**, 331–353 (2018).
56. H. Päivä *et al*., High-dose statins and skeletal muscle metabolism in humans: A randomized, controlled trial. *Clin. Pharmacol. Ther.* **78**, 60–68 (2005).
57. H. A. J. Stringer, G. K. Sohi, J. A. Maguire, H. C. F. Côté, Decreased skeletal muscle mitochondrial DNA in patients with statin-induced myopathy. *J. Neurol. Sci.* **325**, 142–147 (2013).
58. A. Cirigliano *et al*., Statins interfere with the attachment of S. cerevisiae mtDNA to the inner mitochondrial membrane. *J. Enzyme Inhib. Med. Chem.* **35**, 129–137 (2020).
59. S. Z. Yoo *et al*., Role of exercise in age-related sarcopenia. *J. Exerc. Rehabil.* **14**, 551–558 (2018).
60. N. T. Theilen, G. H. Kunkel, S. C. Tyagi, The role of exercise and TFAM in preventing skeletal muscle atrophy. *J. Cell. Physiol.* **232**, 2348–2358 (2017).
61. N. T. Theilen, N. Jeremic, G. J. Weber, S. C. Tyagi, TFAM overexpression diminishes skeletal muscle atrophy after hindlimb suspension in mice. *Archiv. Biochem. Biophys.* **666**, 138–147 (2019).
62. J. P. Leduc-Gaudet, O. Reynaud, S. N. Hussain, G. Gouspillou, Parkin overexpression protects from ageing-related loss of muscle mass and strength. *J. Physiol.* **597**, 1975–1991 (2019).
63. L. Ranvier, Proprietés et structures differentes des muscles rouges et des muscles blanc, chez les lapins et chez les raises. *CR Hebd Acad. Sci.* **77**, 1030–1043 (1873).
64. T. Ogata, Y. Yamasaki, Scanning electron-microscopic studies on the three-dimensional structure of mitochondria in the mammalian red, white and intermediate muscle fibers. *Cell Tissue Res.* **241**, 251–256 (1985).
65. L. He *et al*., Detection and quantification of mitochondrial DNA deletions in individual cells by real-time PCR. *Nucleic Acids Res.* **30**, e68 (2002).
66. L. Larsson, Histochemical characteristics of human skeletal muscle during aging. *Acta Physiol. Scand.* **117**, 469–471 (1983).
67. J. Wanagat, Z. Cao, P. Pathare, J. M. Aiken, Mitochondrial DNA deletion mutations colocalize with segmental electron transport system abnormalities, muscle fiber atrophy, fiber splitting, and oxidative damage in sarcopenia. *FASEB J.* **15**, 322–332 (2001).
68. A. Herbst *et al*., Latent mitochondrial DNA deletion mutations drive muscle fiber loss at old age. *Aging Cell* **15**, 1132–1139 (2016).
69. M. Picard, D. Ritchie, M. M. Thomas, K. J. Wright, R. T. Hepple, Alterations in intrinsic mitochondrial function with aging are fiber type-specific and do not explain differential atrophy between muscles. *Aging Cell* **10**, 1047–1055 (2011).
70. J. D. Murray, *Interdisciplinary Applied Mathematics, Mathematical Biology* , Mathematical Biology: I. An Introduction (Springer-Verlag, New York, ed. 3, 2002).
71. Z. Cao, J. Wanagat, S. H. McKiernan, J. M. Aiken, Mitochondrial DNA deletion mutations are concomitant with ragged red regions of individual, aged muscle fibers: Analysis by laser-capture microdissection. *Nucleic Acids Res.* **29**, 4502–4508 (2001).
72. F. J. Miller, F. L. Rosenfeldt, C. Zhang, A. W. Linnane, P. Nagley, Precise determination of mitochondrial DNA copy number in human skeletal and cardiac muscle by a PCR-based assay: Lack of change of copy number with age. *Nucleic Acids Res.* **31**, e61 (2003).
73. R. Shenkar *et al*., The mutation rate of the human mtDNA deletion mtDNA4977. *Am. J. Hum. Genet.* **59**, 772 (1996).
74. G. López-Lluch *et al*., Calorie restriction induces mitochondrial biogenesis and bioenergetic efficiency. *Proc. Natl. Acad. Sci.* **103**, 1768–1773 (2006).
75. A. E. Civitarese *et al*., Calorie restriction increases muscle mitochondrial biogenesis in healthy humans. *PLoS Med.* **4**, e76 (2007).
76. N. A. Khan *et al*., Effective treatment of mitochondrial myopathy by nicotinamide riboside, a vitamin b 3. *EMBO Mol. Med.* **6**, 721–731 (2014).
77. E. Pirinen *et al*., Niacin cures systemic nad+ deficiency and improves muscle performance in adult-onset mitochondrial myopathy. *Cell Metabol.* **31**, 1078–1090 (2020).
78. A. B. Knott, G. Perkins, R. Schwarzenbacher, E. Bossy-Wetzel, Mitochondrial fragmentation in neurodegeneration. *Nat. Rev. Neurosci.* **9**, 505–518 (2008).
79. M. N. Serasinghe, J. E. Chipuk, *Pharmacology of Mitochondria*. , Mitochondrial fission in human pp. 159–188.(2016).
80. A. Terman, T. Kurz, M. Navratil, E. A. Arriaga, U. T. Brunk, Mitochondrial turnover and aging of long-lived postmitotic cells: The mitochondrial-lysosomal axis theory of aging. *Antioxid. Redox Signal.* **12**, 503–535 (2010).
81. R. Filograna, M. Mennuni, D. Alsina, N. G. Larsson, Mitochondrial DNA copy number in human disease: The more the better?. *FEBS Lett.* **595**, 976–1002 (2021).
82. J. U. Kreft, Biofilms promote altruism. *Microbiology* **150**, 2751–2760 (2004).
83. B. Houchmandzadeh, M. Vallade, Selection for altruism through random drift in variable size populations. *BMC Evol. Biol.* **12**, 61 (2012).
84. S. Okasha, Biological Altruism, The Stanford Encyclopedia of Philosophy in E. N. Zalta, Ed. (Metaphysics Research Lab, Stanford University, 2020). Summer 2020 edition.
85. T. L. Schwarz, Mitochondrial trafficking in neurons. *Cold Spring Harb. Perspect. Biol.* **5**, a011304 (2013).
86. D. Torralba, F. Baixauli, F. Sánchez-Madrid, Mitochondria know no boundaries: Mechanisms and functions of intercellular mitochondrial transfer. *Front. Cell Dev. Biol.* **4**, 107 (2016).
87. A. Ammerman, L. Cavalli-Sforza, *Transformations: Mathematical Approaches to Culture Change* , The wave of advance model for the spread of early farming (Academic Press, New York, pp. 275–293. 1979).
88. A. J. Robson, A bioeconomic view of the neolithic transition to agriculture. *Can. J. Econ. Revue canadienne d'économique* **43**, 280–300 (2010).
89. I. G. Johnston, B. C. Rickett, N. S. Jones, Explicit tracking of uncertainty increases the power of quantitative rule-of-thumb reasoning in cell biology. *Biophys. J.* **107**, 2612–2617 (2014).